# Silver Nanowire Embedded in P3HT: PCBM for High-Efficiency Hybrid Photovoltaic Device Applications

**Chul-Hyun Kim,[†,§] Sang-Ho Cha,[∥,§] Sung Chul Kim,[†] Myungkwan Song,[†] Jaebeom Lee,[‡] Won Suk Shin,[⊥] Sang-Jin Moon,[⊥] Joong Hwan Bahng,[#] Nicholas A. Kotov,[∥,*] and Sung-Ho Jin[†,*]**

[†]Department of Chemistry Education, Interdisciplinary Program of Advanced Information and Display Materials, Pusan National University, Busan, 609-735, Korea, [‡]Department of Nanomedical Engineering, Pusan National University, Miryang, 627-706, Korea, [⊥]Korea Research Institute of Chemistry Technology, 100 Jang-dong, Yuseong-gu, Daejeon 305-343, Korea, and [∥]Department of Chemical Engineering and [#]Department of Biomedical Engineering, University of Michigan, Ann Arbor, Michigan 48109, United States. [§] These authors contributed equally to this paper.

**ABSTRACT** A systematic approach has been followed in the development of a high-efficiency hybrid photovoltaic device that has a combination of poly(3-hexylthiophene) (P3HT), [6,6]-phenyl C61-butyric acid methyl ester (PCBM), and silver nanowires (Ag NWs) in the active layer using the bulk heterojunction concept. The active layer is modified by utilizing a binary solvent system for blending. In addition, the solvent evaporation process after spin-coating is changed and an Ag NWs is incorporated to improve the performance of the hybrid photovoltaic device. Hybrid photovoltaic devices were fabricated by using a 1:0.7 weight ratio of P3HT to PCBM in a 1:1 weight ratio of *o*-dichlorobenzene and chloroform solvent mixture, in the presence and absence of 20 wt % of Ag NWs. We also compared the photovoltaic performance of Ag NWs embedded in P3HT:PCBM to that of silver nanoparticles (Ag NPs). Atomic force microscopy, scanning electron microscopy, transmittance electron microscopy, UV–visible absorption, incident photon-to-current conversion efficiency, and time-of-flight measurements are performed in order to characterize the hybrid photovoltaic devices. The optimal hybrid photovoltaic device composed of Ag NWs generated in this effort exhibits a power conversion efficiency of 3.91%, measured by using an AM 1.5G solar simulator at 100 mW/cm$^2$ light illumination intensity.

**KEYWORDS:** hybrid photovoltaic device · Ag nanowires · integragted photocurrent density · P3HT · PCBM

Organic photovoltaic devices (OPVs) possess great potential as renewable and alternative sources of electrical energy.[1−4] The demand for inexpensive renewable energy sources is the driving force behind new approaches to the development of low-cost photovoltaic devices. In the last couple of years, an intense effort has been given to the development of viable and high-efficiency OPVs. Particular attention has focused on methods to construct the donor–acceptor bilayer,[5] commonly achieved by using vacuum deposition of molecular components.[6] In addition, the so-called bulk heterojunction (BHJ) concept has been explored.[7] The BHJ is represented in the ideal case as a bicontinuous composite of an electron donor and electron acceptor phase, in which the interfacial area between the electron donor and acceptor is maximized. The development of interpenetrating electron donor–acceptor conjugated polymer-based BHJ OPVs, such as polymer:fullerene, polymer:polymer, and polymer:nanocrystal, made it possible to reach high power conversion efficiency (PCE).

The combination of regioregular P3HT and PCBM can be used in polymer-based OPVs that combine electron donor and electron acceptor materials, which showed a PCE of up to ∼5.0%.[8−10] For ideal performance, polymer-based OPVs should fulfill several other requirements, including efficient absorption of sunlight, excellent charge carrier generation, transport, and collection, and high stability. To attain these properties, hybrid photovoltaic devices have been designed that combine blends of conjugated polymers with *n*-type inorganic nanomaterials, in order to take advantage of enhanced light absorption, high charge carrier mobility, and excellent chemical and physical stability seen with inorganic semiconductors. The hybrid system has opened new opportunities for the development of future generation photovoltaic devices and new device technologies and a platform to study three-dimensional morphology. Several hybrid photovoltaic devices that employ CdS,[11] ZnO,[12] CdSe,[13,14] CdTe,[15] and $TiO_2$ nanoparticles[16] have been reported. Metal nanomaterials, such as those of silver (Ag) and gold (Au), possess localized surface plasmon resonance (LSPR)[17−19] that exhibits resonance light absorption in the visible region. For instance, Olsen reported a P3HT/ZnO nanorod cell exhibiting a short-circuit current density ($J_{sc}$) of 2.2 mA/cm$^2$, an open-circuit voltage ($V_{oc}$) of 0.44 V, a fill factor (FF)

* Address correspondence to kotov@umich.edu (N.A.K.), shjin@pusan.ac.kr (S.-H.J.).

Received for review February 4, 2011 and accepted March 25, 2011.

**Published online March 26, 2011**
**10.1021/nn200469d**

of 0.56, and an PCE of 0.53%.[20] They also reported that the introduction of PCBM into the hybrid photovoltaic devices could significantly improve the PCE of the devices up to 2.03%. Despite impressive progress in the development of hybrid photovoltaic devices, the PCE is still relatively low (below 3%). In our research in this area, we have previously reported novel low-band gap polymers and novel hybrid polymer photovoltaic device made by generating Ag nanoparticles (NPs) in polymer:fullerene BHJ structures.[21−26] Of particular relevance to the investigation described below are one-dimensional (1D) nanowires, which have highly unique electronic and optical properties.[27−29] Ag nanowires (Ag NWs) with well-defined dimensions represent a particularly interesting class of nanostructures because bulk Ag exhibits the highest electrical and thermal conductivity among all metals. As an extension of our work, in this article, we report the highly efficient hybrid photovoltaic devices by using the synergistic effects between P3HT:PCBM-based OPVs and Ag NWs as a doped electron acceptor for offering direct pathways for electric conduction by randomly mixing the P3HT and PCBM in the presence or absence of 20 wt % Ag NWs (Figure 1). The highest PCE of the hybrid photovoltaic device prepared in this manner is 3.91% using an AM 1.5G solar simulator (Oriel 300 W) at a 100 mW/cm$^2$ light illumination intensity. The results were correlated with the morphology of active layers, which was characterized by using atomic force microscopy (AFM), field emission scanning electron microscopy (FE-SEM), transmittance electron microscopy (TEM), and time-of-flight (TOF) measurements. In addition, the characteristics of the hybrid photovoltaic device are consistent with the balance of charge carrier mobility, along with incident photon-to-current conversion efficiency (IPCE), and UV−visible absorption spectroscopic properties.

## RESULTS AND DISCUSSION

The hybrid photovoltaic device with P3HT:PCBM:Ag NWs as an active layer was designed on the basis of the following considerations: (i) using the highly efficient OPVs based on P3HT:PCBM, (ii) slight doping of the electron acceptor such as Ag NWs to improve the photovoltaic performance of hybrid photovoltaic devices, and (iii) in order to reduce the number of interparticle hopping events, using elongated Ag NWs in combination with P3HT:PCBM instead of Ag NPs.

Figure 2 shows the UV−visible absorption spectra of P3HT:PCBM, P3HT:PCBM:Ag NWs, and P3HT:PCBM:Ag NPs for comparison. The films were prepared by employing the spin-coating technique and then air-dried without thermal annealing. Encouraging results showed that the Ag NWs embedded in P3HT:PCBM matrix improved the optical absorption in comparison with P3HT:PCBM and P3HT:PCBM:Ag NPs. Both films show characteristic

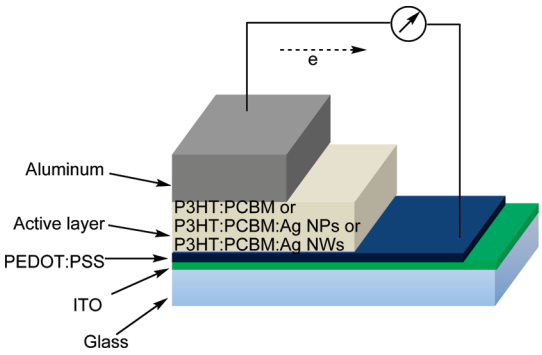


**Figure 1. Device structure used for fabrication of the photovoltaic device.**

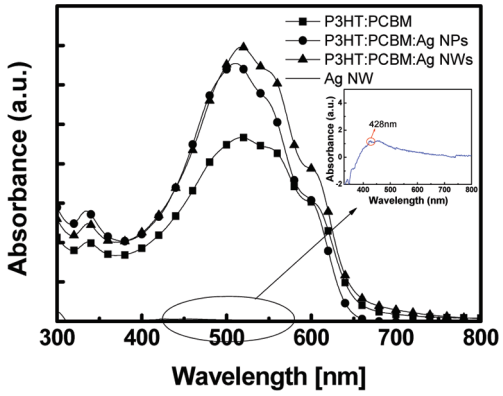


**Figure 2. UV−visible absorption spectra of active layers (P3HT:PCBM, P3HT:PCBM:Ag NPs, P3HT:PCBM:Ag NWs, and Ag NWs). Inset: UV−visible absorption spectrum of Ag NWs in solution state.**

maxima for P3HT in the 400−650 nm region and for PCBM at *ca.* 330 nm. In the spectral range of 330−650 nm, where the P3HT:PCBM blend film is absorbing, enhanced optical absorption was observed due to the increased electric field in the active layer by excited LSPR and scattering effects around the Ag NWs through homogeneous networking among organic and inorganic materials.[30−32] This result corresponds to about 20% increase of the total optical absorption of the devices in the spectral range 330−650 nm. In liquid state, the UV−visible absorption spectrum of Ag NWs showed a characteristic peak at 428 nm, as shown in the inset of Figure 2. The Ag NWs exhibit a strong absorption peak at around 428 nm, which is a well-known surface plasmon resonance (SPR) absorption of Ag NWs in solution state.[33] The absorption band at around 428 nm is due to the collective oscillation of all free electrons in the Ag NWs resulting from the interaction with electromagnetic radiation. The electric field of the incoming radiation induces the formation of a dipole in the NWs. Therefore, the increase of total optical absorption induced by SPR of Ag NWs implies that Ag NWs in the active layer potentially lead to high efficiency for the formation of an exciton through the increase of the effective optical path length of incident light[34] and enhancement of local optical field on the surface of Ag NWs.[32]

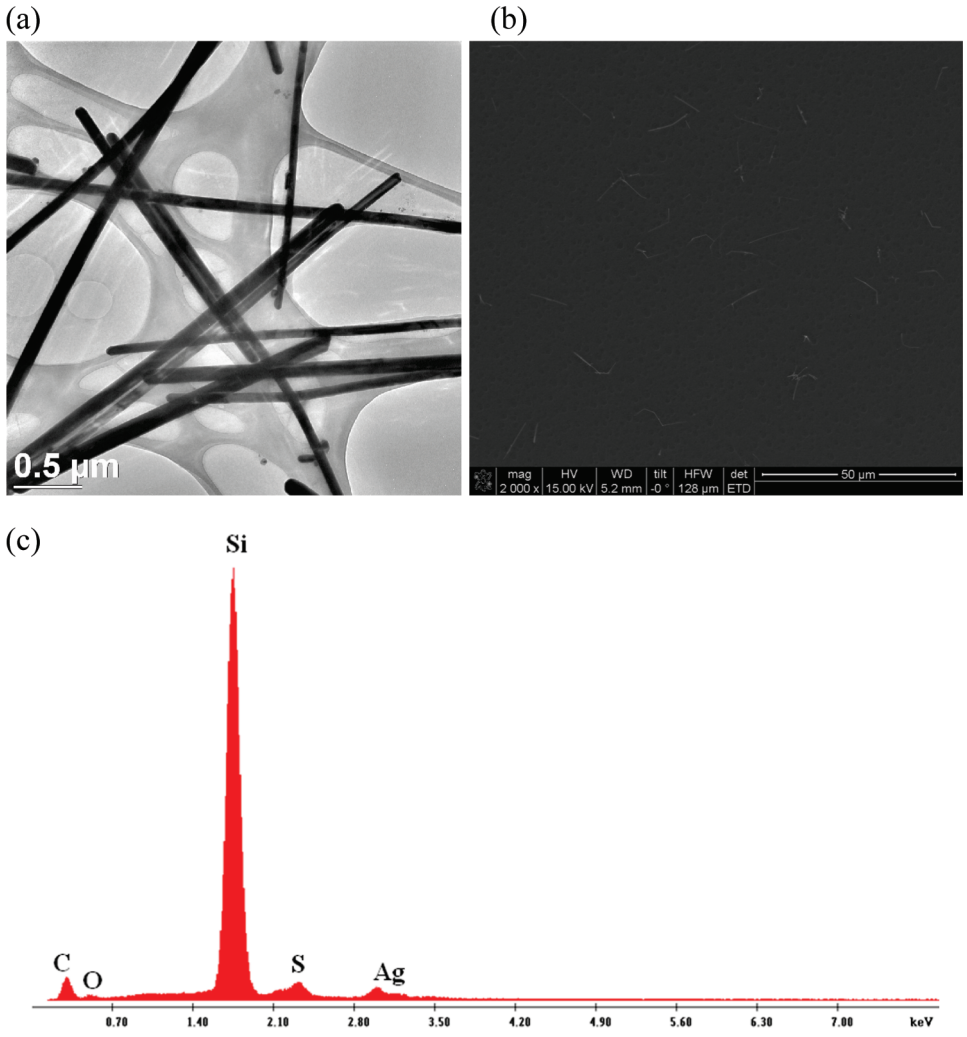


**Figure 3. (a) TEM and (b) SEM micrographs and (c) representative EDAX spectrum of the active layer of P3HT:PCBM:Ag NWs.**

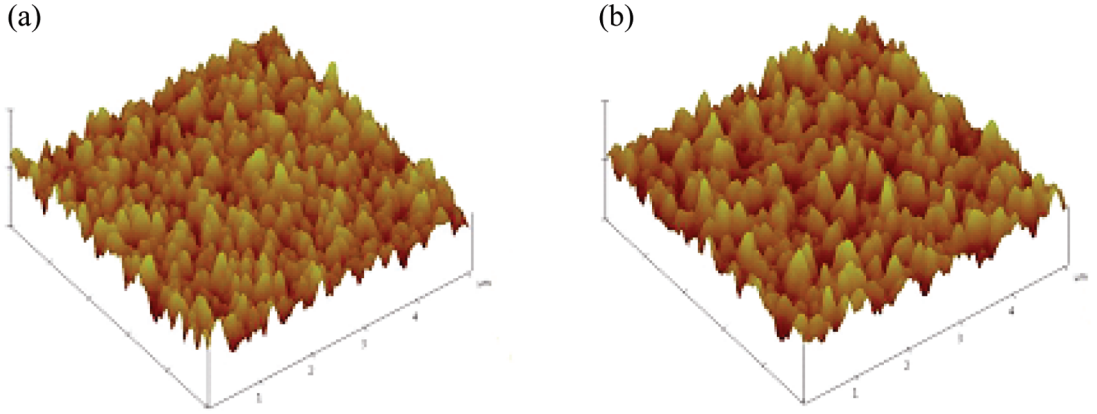


**Figure 4. AFM micrographs of active layers produced from P3HT:PCBM (a) and P3HT:PCBM:Ag NWs (b). The rms roughnesses over the 5 $\mu$m $\times$ 5 $\mu$m areas are 6.7 and 8.7 nm, respectively.**

TEM and SEM images for the active layer of P3HT:PCBM:Ag NWs reveal that the Ag NWs used in this study have a diameter and length of *ca.* 110 nm and *ca.* 5.0−8.0 $\mu$m, respectively, and are homogeneously distributed all over the matrix of P3HT and PCBM (Figure 3a and b). The homogeneous distribution of Ag NWs in the active layer is further supported by the result of EDAX analysis, as shown in Figure 3c. To explore the morphology of active layer films with the following configuration of ITO/PEDOT:PSS/active layer/Al (Figure 1) using P3HT:PCBM and P3HT:PCBM:Ag NWs as active layer, the Al cathode was removed by using

sticky tape after thermal annealing.[35] AFM measurements were then carried out, yielding the tapping-mode images as shown in Figure 4. Inspection of the images shows that an extremely smooth surface is present in both the P3HT:PCBM and P3HT:PCBM:Ag NWs films. However, careful analysis showed that the root-mean-square (rms) values for the P3HT:PCBM and P3HT:PCBM:Ag NWs films are 6.7 and 8.7 nm, respectively. The larger roughness observed for the P3HT:PCBM:Ag NWs film could be a consequence of the presence of the Ag NWs in the P3HT:PCBM active layer.

The hybrid photovoltaic devices were optimized by using different weight ratios of P3HT, PCBM, and Ag NW content and varying the active layer thicknesses. Due to the diameter of Ag NWs, the optimal active layer thickness of the photovoltaic devices were found to be 140−150 nm, containing an active layer composed of either P3HT:PCBM (device 1), P3HT:PCBM:Ag NPs (device 2), or P3HT:PCBM:Ag NWs (device 3) with a mask. The current density−voltage ($J$−$V$) curves of these photovoltaic devices are displayed in Figure 5, and the photovoltaic performances are summarized in Table 1. All of the photovoltaic devices have nearly the same $V_{oc}$ at one sun intensity (100 mW/cm$^2$) under simulated AM 1.5G illumination. However, the comparison of devices 1, 2, and 3 shows that $J_{sc}$ of the photovoltaic device of P3HT:PCBM:Ag NWs (9.32 mA/cm$^2$) is larger than that of devices of P3HT:PCBM (8.47 mA/cm$^2$) and P3HT:PCBM:Ag NPs (9.28 mA/cm$^2$). This likely results from the fact that Ag NWs cause an enhancement in the light absorption ability and high and balanced charge carrier mobility of the device of P3HT:PCBM:Ag NWs.[36] By reducing the number of interparticle hopping events, using Ag NWs instead of Ag NPs randomly dispersed in a P3HT:PCBM, can result in improved electron transport in the blended films; thus the PCE will be further improved. Increased electrical conductivity leads to an increase in $J_{sc}$ and, consequently, to an increase in the PCE of the hybrid photovoltaic device (3.91% compared to 3.31% and 3.56% for the photovoltaic devices of P3HT:PCBM and P3HT:PCBM:Ag NPs).

The drop-casting technique, involving slow drying of the films in a solvent-saturated atmosphere, had to be used instead of spin-coating to achieve sufficiently thick films for TOF measurements. Carrier mobility ($\mu$) can be determined from the TOF data from the relationship $\mu = d^2/Vt_{tr}$, where $V$ is the applied bias, $d$ is the thickness of the active layer film, and $t_{tr}$ is the transit time. For nondispersive charge transport, the transit time corresponds to the inflection point in the decay of the current from its plateau value. For dispersive transients, the transit time is the intercept of the pre- and post-transit asymptotes of double logarithmic plots of the photocurrent. It has been reported that electron mobility is faster than hole mobility in disordered systems, such as $\pi$-conjugate polymers, that show highly dispersive current transients.[37] Figure 6 shows plots of the mobilities of the P3HT:PCBM and P3HT:PCBM:Ag NWs films as a function of the electrical field at room temperature, and the characteristic data

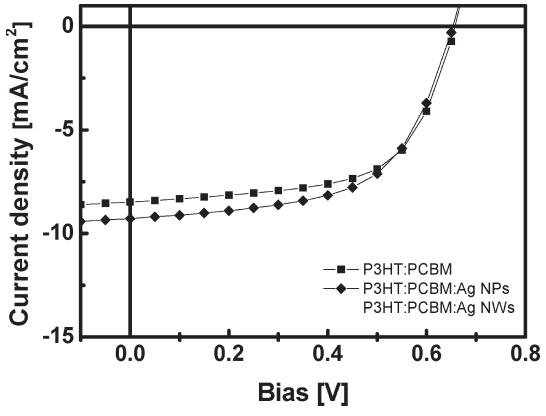


**Figure 5. Current density−voltage ($J$−$V$) curves for P3HT:PCBM, P3HT:PCBM:Ag NPs, and P3HT:PCBM:Ag NWs (AM 1.5G condition with incident light power intensity of 100 mW/cm$^2$).**

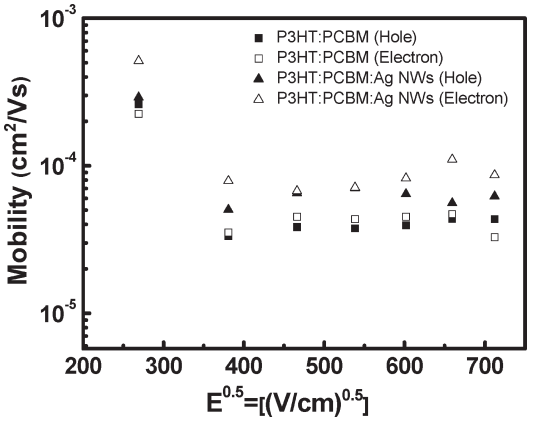


**Figure 6. Field dependence of the hole and electron mobility for P3HT:PCBM and P3HT:PCBM:Ag NWs.**

**TABLE 1. Performance of P3HT:PCBM, P3HT:PCBM:Ag NPs, and P3HT:PCBM:Ag NWs Photovoltaic Devices under AM 1.5G Illumination (100 mW/cm$^2$)**

| device | $V_{oc}$ (V) | $J_{sc}$ (mA/cm$^2$) | integrated photocurrent[a] (mA/cm$^2$) | FF (%) | PCE (%) | $R_{Sh}$ (Ω cm$^2$) | $R_S$ (Ω cm$^2$) |
|---|---|---|---|---|---|---|---|
| P3HT:PCBM | 0.65 | 8.47 | 8.25 | 60.1 | 3.31 | 682.3 | 12.32 |
| P3HT:PCBM:Ag NPs | 0.65 | 9.28 | 9.09 | 59.1 | 3.56 | 632.9 | 13.18 |
| P3HT:PCBM:Ag NWs | 0.66 | 9.32 | 9.28 | 63.6 | 3.91 | 870.2 | 11.62 |

[a] Integrated photocurrent obtained by integrating the curves shown in Figure 8a.

**TABLE 2. Charge Carrier Transport Parameters of P3HT:PCBM and P3HT:PCBM:Ag NWs**

| | mobility | | | | | |
|---|---|---|---|---|---|---|
| | P3HT:PCBM | | | P3HT:PCBM:Ag NWs | | |
| electrical field $(V/cm)^{0.5}$ | hole ($\mu_h$, $cm^2/(V\ s)$) | electron ($\mu_e$, $cm^2/(V\ s)$) | $\mu_e/\mu_h$ | hole ($\mu_h$, $cm^2/(V\ s)$) | electron ($\mu_e$, $cm^2/(V\ s)$) | $\mu_e/\mu_h$ |
| 269 | $2.61 \times 10^{-4}$ | $2.25 \times 10^{-4}$ | 0.862 | $2.91 \times 10^{-4}$ | $5.15 \times 10^{-4}$ | 1.770 |
| 380 | $3.34 \times 10^{-5}$ | $3.53 \times 10^{-5}$ | 1.057 | $5.04 \times 10^{-5}$ | $7.91 \times 10^{-5}$ | 1.569 |
| 466 | $3.84 \times 10^{-5}$ | $4.50 \times 10^{-5}$ | 1.172 | $6.53 \times 10^{-5}$ | $6.76 \times 10^{-5}$ | 1.035 |
| 538 | $3.77 \times 10^{-5}$ | $4.35 \times 10^{-5}$ | 1.154 | $7.07 \times 10^{-5}$ | $7.13 \times 10^{-5}$ | 1.008 |
| 602 | $3.95 \times 10^{-5}$ | $4.51 \times 10^{-5}$ | 1.142 | $6.44 \times 10^{-5}$ | $8.23 \times 10^{-5}$ | 1.278 |
| 659 | $4.38 \times 10^{-5}$ | $4.70 \times 10^{-5}$ | 1.073 | $5.57 \times 10^{-5}$ | $1.10 \times 10^{-4}$ | 1.975 |
| 712 | $4.36 \times 10^{-5}$ | $3.28 \times 10^{-5}$ | 0.752 | $6.21 \times 10^{-5}$ | $8.64 \times 10^{-5}$ | 1.391 |

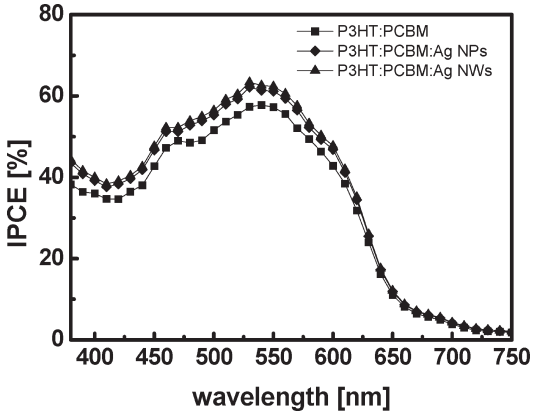


**Figure 7. Incident photon-to-current conversion efficiencies (IPCE) of P3HT:PCBM, P3HT:PCBM:Ag NPs, and P3HT:PCBM:Ag NWs.**

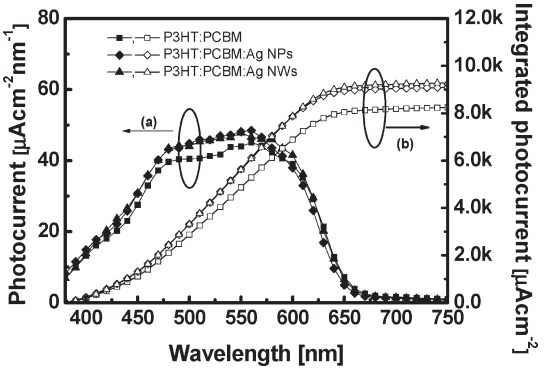


**Figure 8. (a) Photocurrents obtained using data from Figure 7. (b) Total solar photocurrent obtained by integrating the curves shown in plots (a).**

are summarized in Table 2. The results show that the hole and electron mobilities for P3HT:PCBM film are *ca.* $\mu_h = 3.34 \times 10^{-5}\ cm^2\ V^{-1}\ s^{-1}$ and $\mu_e = 3.53 \times 10^{-5}\ cm^2\ V^{-1}\ s^{-1}$, respectively, at $E^{0.5} = 380\ (V\ cm^{-1})^{0.5}$. For the P3HT:PCBM:Ag NWs film, the hole and electron mobilities are increased to $\mu_h = 5.04 \times 10^{-5}\ cm^2\ V^{-1}\ s^{-1}$ and $\mu_e = 7.91 \times 10^{-5}\ cm^2\ V^{-1}\ s^{-1}$, respectively, at $E^{0.5} = 380\ (V\ cm^{-1})^{0.5}$. In general, the P3HT:PCBM:Ag NWs film has a 1.5 times larger $\mu_e/\mu_h$ as compared to the P3HT:PCBM film. The change in the hybrid photovoltaic device is attributed to the presence of Ag NWs, which leads to an increase in PCE.

A very useful parameter for determining the PCE of photovoltaic devices is the IPCE, which reaches 100% when all incident photons generate electron–hole pairs. However, in practical situations, IPCE is typically less than 100% as a result of losses caused by the reflection of incident photons, imperfect absorption of photons by the semiconductor, and recombination of charge carriers within the semiconductor. IPCE spectra for the photovoltaic devices of P3HT:PCBM, P3HT:PCBM:Ag NPs, and P3HT:PCBM:Ag NWs are displayed in Figure 7. Although all IPCE spectra are similar in shape, the IPCE values for the photovoltaic devices containing P3HT:PCBM:Ag NWs are higher than ones for the P3HT:PCBM and P3HT:PCBM:Ag NPs in all wavelength. For example, the photovoltaic device of P3HT:PCBM was found to have an IPCE maximum of 57% at 540 nm and the IPCE of the hybrid photovoltaic device with P3HT:PCBM:Ag NWs is 63% at the same wavelength. The difference is a consequence of the increased charge carrier mobility and, thus, the improved absorption of the P3HT:PCBM:Ag NWs active layer. Integrated photocurrent curves were obtained by using integrated IPCE spectra (Figure 8b). The integrated photocurrent densities of the photovoltaic devices of P3HT:PCBM, P3HT:PCBM:Ag NPs, and P3HT:PCBM:Ag NWs are 8.25, 9.09, and 9.28 $mA/cm^2$, respectively. These values are in good agreement with the measured photocurrent densities of 8.47, 9.28, and 9.32 $mA/cm^2$, respectively. In this study, the error between measured $J_{sc}$ and integrated photocurrent was *ca.* 5%, which is in the 5–10% range often seen in these values.[38] Comparisons of the integrals of the calculated photocurrent densities with those of photocurrent densities from a solar simulator are summarized in Table 1. These slight differences are also a consequence of the spectral mismatch of the xenon lamp, which exhibits a higher photon flux than the sun in the UV region.[39]

## CONCLUSIONS

The studies described above have led to the fabrication of the first, highly efficient bulk heterojunction

hybrid photovoltaic device with P3HT:PCBM:Ag NWs. Investigations of the morphology of the active layer in the photovoltaic device by AFM, FE-SEM, TEM, and EDAX show that an Ag NW is embedded in the P3HT:PCBM films. The P3HT:PCBM, P3HT:PCBM:Ag NPs, and P3HT:PCBM:Ag NWs based on photovoltaic devices have nearly the same $V_{oc}$ values of 0.65 V at one sun intensity (100 mW/cm$^2$) simulated with AM 1.5G illumination. The fabricated hybrid photovoltaic device has reasonably high $J_{sc}$, FF, and PCE values of 9.32 mA/cm$^2$, 63.6, and 3.91%, respectively. It is anticipated that the strategy presented above for constructing polymer:fullerene:inorganic hybrid photovoltaic devices will be generally applicable to the design and fabrication of other OPVs with improved PCE values.

## EXPERIMENTAL SECTION

**Fabrication and Evaluation of Photovoltaic Devices.** P3HT was used as supplied. PCBM, Ag NPs, and Ag NWs solutions were prepared according to the procedure published earlier.[25,40,41] The organic−inorganic hybrid photovoltaic devices, using P3HT as the electron donor and PCBM, Ag NPs, and Ag NWs as the acceptor, were fabricated to have the following simple structure: ITO/PEDOT:PSS/P3HT:PCBM/Al, ITO/PEDOT:PSS/P3HT:PCBM:Ag NPs/Al, and ITO/PEDOT:PSS/P3HT:PCBM:Ag NWs/Al. Indium−tin-oxide (ITO)-coated glass, cleaned ultrasonically with detergent followed by distilled water, acetone, and 2-propanol sequentially, was used as transparent electrode. The ITO surface was modified by spin-coating of a 40 nm thick, highly reactive, PEDOT:PSS (CLEVIOS PH) layer after exposing the ITO surface to ozone for 15 min. The PEDOT:PSS layer was dried on a hot plate in air for 30 min at 150 °C. The cosolvent system was prepared by mixing a 1:1 weight ratio of *o*-dichlorobenzene and chloroform. The P3HT:PCBM (pristine) blend at 1:0.7 weight ratio and P3HT:PCBM:Ag NPs or Ag NWs (hybrid) solutions were prepared and allowed to stir for 24 h. To form the hybrid solution, Ag NPs or Ag NWs were added to the pristine solution (20 wt % with respect to the weight of P3HT:PCBM). The active layer was spin-coated from these blend solutions over the dried PEDOT:PSS layer at room temperature, and the thickness was maintained at 140−150 nm. Thicknesses of the thin films were measured using a KLA Tencor Alpha-step IQ surface profilometer with an accuracy of ±1 nm. The active layer was dried at room temperature for 30−40 min. After drying the active layer, the photovoltaic devices were charged into the thermal evaporator through a glovebox and Al metal (150 nm) was deposited as the cathode under a vacuum of less than $5 \times 10^{-6}$ Torr, which yields a 9 mm$^2$ active area per each pixel. After depositing the Al cathode, the photovoltaic devices were removed from the thermal chamber and thermally annealed on a hot plate at 150 °C for 30 min inside the glovebox. The performance of the photovoltaic cells was measured using a calibrated AM 1.5G solar simulator (Oriel 300 W) at a 100 mW/cm$^2$ light intensity adjusted with a standard PV reference cell (2 cm × 2 cm monocrystalline silicon solar cell, calibrated at NREL, Colorado, USA). After current density−voltage (*J*−*V*) curves were recorded using a standard source measurement unit (Keithley 236), immediately, the incident photon-to-electron conversion efficiency was measured by interposing a monochromator between the xenon lamp and the photovoltaic cell. The incident photon current density of the photovoltaic cell and incident power density of light for each of the wavelengths (380−750 nm) was measured using a Keithley 236 and a light power meter. Then, the IPCE was calculated as a function of all measured parameters. All fabrication steps and characterization measurements were performed in an ambient environment without a protective atmosphere.

**Measurement of Mobility.** We fabricated a TOF sample for hole and electron mobility measurements. The active layer was spin-coated from P3HT:PCBM and P3HT:PCBM:Ag NWs blend solutions on a cleaner ITO-coated glass substrate, and the active layer had a typical thickness of 1.3 $\mu$m. After the active layer was sufficiently dried in air, we deposited an Al electrode by thermal evaporation and thermally annealed it at 150 °C for 30 min inside the glovebox. TOF measurements were performed using a VSL-337ND-S nitrogen laser ($\lambda$ = 337 nm) and recorded by a digital oscilloscope (LeCroy).

**Imaging.** AFM images were acquired with a Digital Instrument Nanoscope 3D ADC5, Mutimode (Veeco Instruments Inc., CA), in tapping mode. Samples for AFM image measurement were fabricated by first spin-coating a PEDOT:PSS layer on top of ITO-coated glass substrates and then drying at room temperature under air. The active layer was spin-coated on top of the PEDOT:PSS layer. The samples' structures for AFM imaging of surface morphology were ITO/PEDOT:PSS/P3HT:PCBM and ITO/PEDOT:PSS/P3HT:PCBM:Ag NWs. The SEM image was taken by a FEI Nova Nanolab dualbeam FIB and scanning electron microscope with EDAX UTW detector. The films were prepared in a manner identical to that for AFM measurement. TEM was conducted with a JEOL 2010F electron microscope.

**Absorption Spectroscopy.** UV−visible absorption spectra were recorded on a V-570 model UV−visible−near IR spectrophotometer (JASCO). P3HT:PCBM, P3HT:PCBM:Ag NPs, and P3HT:PCBM:Ag NWs blend films for absorption measurements were spin-coated on Quartz glass and then dried in air for 30 min without heat treatment.

*Acknowledgment.* This investigation was supported financially by the New & Renewable Energy Program of the Korea Institute of Energy Technology Evaluation and Planning (KETEP) grant (No. 20103020010050) funded by the Ministry of Knowledge Economy, and a National Research Foundation of Korea (NRF) grant funded by the Ministry of Education, Science and Technology (MEST) (No. M10600000157-06J0000-15710), and the cooperative R&D Program funded by the Korea Research Council Industrial Science and Technology, Republic of Korea. N. A.K. acknowledges the Center for Solar and Thermal Energy Conversion, an Energy Frontier Research Center funded by the U.S. Department of Energy, Office of Science, Office of Basic Energy Sciences, under Award No. #DE-SC0000957.

## REFERENCES AND NOTES

1. Sariciftci, N. S.; Smilowitz, L.; Heeger, A. J.; Wudl, F. Photoinduced Electron Transfer from a Conducting Polymer to Buckminsterfullerene. *Science* **1992,** *258*, 1474–1476.
2. Yu, G.; Gao, J.; Hummelen, J. C.; Wudl, F.; Heeger, A. J. Polymer Photovoltaic Cells: Enhanced Efficiencies via a Network of Internal Donor-Acceptor Heterojunctions. *Science* **1995,** *270*, 1789–1791.
3. Brunetti, F. G.; Kumar, R.; Wudl, F. Organic Electronics from Perylene to Organic Photovoltaics: Painting a Brief History with a Broad Brush. *J. Mater. Chem.* **2010,** *20*, 2934–2948.
4. Cai, W.; Gong, X.; Cao, Y. Polymer Solar Cells: Recent Development and Possible Routes for Improvement in the Performance. *Sol. Energy Mater. Sol. Cells* **2010,** *94*, 114–127.
5. Xue, J.; Uchida, S.; Rand, B. P.; Forrest, S. R. 4.2% Efficient Organic Photovoltaic Cells with Low Series Resistances. *Appl. Phys. Lett.* **2004,** *84*, 3013–3015.
6. Peumans, P.; Yakimov, A.; Forrest, S. R. Small Molecular Weight Organic Thin-Film Photodetectors and Solar Cells. *J. Appl. Phys.* **2003,** *93*, 3693–3723.

7. Halls, J. J. M.; Walsh, C. A.; Greenham, N. C.; Marseglia, E. A.; Friend, R. H.; Friend; Moratti, S. C.; Holmes, A. B. Efficient Photodiodes from Interpenetrating Polymer Networks. *Nature* **1995,** *376*, 498–500.
8. Zhang, Y.; Yip, H. L.; Acton, O.; Hau, S. K.; Huang, F.; Jen, A. K.-Y. A Simple and Effective Way of Achieving Highly Efficient and Thermally Stable Bulk-Heterojunction Polymer Solar Cells Using Amorphous Fullerene Derivatives as Electron Acceptor. *Chem. Mater.* **2009,** *21*, 2598–2600.
9. Peet., J.; Kim, J. Y.; Coates, N. E.; Ma, W. L.; Moses, D.; Heeger, A. J.; Bazab, G. C. Efficiency Enhancement in Low-Bandgap Polymer Solar Cells by Processing with Alkane Dithiols. *Nat. Mater.* **2007,** *6*, 497–500.
10. Irwin, M. D.; Buchholz, D. B.; Hains, A. W.; Chang, R. P. H.; Marks, T. J. p-Type Semiconducting Nickel Oxide as an Efficiency-Enhancing Anode Interfacial Layer in Polymer Bulk-Heterojunction Solar Cells. *Proc. Natl. Acad. Sci. U. S. A.* **2008,** *105*, 2783–2787.
11. Guo, Y.; Li, Y.; Xu, J.; Liu, X.; Xu, J.; Lv, J.; Huang, C.; Zhu, M; Cui, S.; Jiang, L.; Liu, H.; Wang, S. Fabrication of Homogeneous Hybrid Nanorod of Organic/Inorganic Semiconductor Materials. *J. Phys. Chem. C* **2008,** *112*, 8223–8228.
12. Lin, Y. Y.; Lee, Y. Y.; Chang, L.; Wu, J. J.; Chen, C. W. The Influence of Interface Modifier on the Performance of Nanostructured ZnO/Polymer Hybrid Solar Cells. *Appl. Phys. Lett.* **2009,** *94*, 0633081–0633083.
13. Huynh, W. U.; Dittmer, J. J.; Alivisatos, A. P. Hybrid Nanorod-Polymer Solar Cells. *Science* **2002,** *295*, 2425–2427.
14. Sun, B. Q.; Snaith, H. J.; Dhoot, A. S.; Westenhoff, S.; Greenham, N. C. Vertically Segregated Hybrid Blends for Photovoltaic Devices with Improved Efficiency. *J. Appl. Phys.* **2005,** *97*, 014914–014916.
15. Kang, Y.; Park, N.; Kim, D. Hybrid Solar Cells with Vertically Aligned CdTe Nanorods and a Conjugated Polymer. *Appl. Phys. Lett.* **2005,** *86*, 113101–113103.
16. Chang, C. H.; Huang, T. K.; Lin, Y. T.; Lin, Y. Y.; Chen, C. W.; Chu, T. H.; Su, W. F. Improved Charge Separation and Transport Efficiency in Poly(3-hexylthiophene)-$TiO_2$ Nanorod Bulk Heterojunction Solar Cells. *J. Mater. Chem.* **2008,** *18*, 2201–2207.
17. Kim., S. S.; Na, S. I.; Jo, J.; Kim, D. Y.; Nah, Y. C. Plasmon Enhanced Performance of Organic Solar Cells using Electrodeposited Ag Nanoparticles. *Appl. Phys. Lett.* **2008,** *93*, 0733071–00733073.
18. Lee, J. H.; Park, J. H.; Kim, J. S.; Lee, D. Y.; Cho, K. High Efficiency Polymer Solar Cells with Wet Deposited Plasmonic Gold Nanodots. *Org. Electron* **2009,** *10*, 416–420.
19. Morfa, A. J.; Rowlen, K. L.; Reilly, T. H.; Romero, M. J.; Lagemaat, J. van de. Plasmon-Enhanced Solar Energy Conversion in Organic Bulk Heterejunction Photovoltaics. *Appl. Phys. Lett.* **2008,** *92*, 0135041–0135043.
20. Olsen, D. C.; Piris, J.; Collins, R. T.; Shaheen, S. E.; Ginley, D. S. Hybrid Photovoltaic Devices of Polymer and ZnO Nanofiber Composites. *Thin Solid Films* **2006,** *496*, 26–29.
21. Shin, W. S.; Jeong, H. H.; Kim, M. K.; Jin, S. H.; Kim, M. R.; Lee, J. K.; Lee, J. W.; Gal, Y. S. Effects of Functional Groups at Perylene Diimide Derivatives on Organic Photovoltaic Device Application. *J. Mater. Chem.* **2006,** *16*, 384–390.
22. Jin, S. H.; Kim, S. C.; Naidu, B. V. K.; Lee, S. K.; Kim, M. R.; Shin, W. S.; Jung, S. J.; Cho, Y. R.; Shim, J. M.; Lee, J. K.; *et al.* Synthesis and Photovoltaic Properties of Novel PPV-Derivatives Tethered with Spirobifluorene Unit for Polymer Solar Cells. *Sol. Energy Mater. Sol. Cells* **2007,** *91*, 460–466.
23. Jin, S. H.; Kim, S. C.; Jung, S. J.; Kim, M. K.; Shin, W. S.; Lee, J. K.; Lee, J. W.; Gal, Y. S. Synthesis and Photovoltaic Properties of a Low-Band-Gap Polymer Consisting of Alternating Thiophene and Benzothiadiazole Derivatives for Bulk-Heterojunction and Dye-Sensitized Solar Cells. *J. Polym. Sci. Part A: Polym. Chem.* **2007,** *45*, 1394–1402.
24. Jin, S. H.; Naidu, B. V. K.; Shin, J. M.; Kim, S. C.; Shin, W. S.; Lee, J. W.; Gal, Y. S. Optimization of Process Parameters for High-Efficiency Polymer Photovoltaic DevicesBased on P3HT:PCBM System. *Sol. Energy Mater. Sol. Cells* **2007,** *91*, 1187–1193.
25. Naidu, B. V. K.; Park, J. S.; Park, S. M.; Lee, E. J.; Yoon, K. J.; Kim, S. C.; Lee, S. J.; Lee, J. W.; Gal, Y. S.; Jin, S. H. Novel Hybrid Polymer Photovoltaics Made by Generating Silver Nanoparticles in Polymer:Fullerene Bulk-Heterojunction Structures. *Sol. Energy Mater. Sol. Cells* **2008,** *92*, 397–401.
26. Park, J. S.; Ryu, T. I.; Song, M.; Yoon, K. J.; Lee, M. J.; Shin, I. A.; Lee, G. D.; Gal, Y. S.; Jin, S. H. Synthesis and Characterization of Fluorene-Based Low-Band Gap Copolymers Containing Propylenedioxythiophene and Benzothiadiazole Derivatives for Bulk Heterojunction Photovoltaic Cell Applications. *J. Polym. Sci. Part A: Polym. Chem.* **2008,** *46*, 6175–6184.
27. Lu, W.; Lieber, C. M. Nanoelectronics from the Bottom Up. *Nat. Mater.* **2007,** *6*, 841–850.
28. Xia, Y.; Yang, P.; Sun, Y. G.; Wu, Y. Y.; Mayer, B.; Gates, B.; Yin, Y.; Kim, F.; Yan, H. One-Dimensional Nanostructures: Synthesis, Characterization, and Applications. *Adv. Mater.* **2003,** *15*, 353–389.
29. Law, M.; Goldberger, J.; Yang, P. Semiconductor Nanowires and Nanotubes. *Annu. Rev. Mater. Res.* **2004,** *34*, 83–122.
30. Schenning, A. P. H. J.; Meijer, E. W. Supramolecular Electronics; Nanowires from Self-Assembled $\pi$-Conjugated Systems. *Chem. Commun.* **2005,** 3245–3258.
31. Yakimov, A.; Forrest, S. R. High Photovoltage Multiple-Heterojunction Organic Solar Cells Incorporating Interfacial Metallic Nanoclusters. *Appl. Phys. Lett.* **2002,** *80*, 1667–1669.
32. Rand, B. P.; Reumans, P.; Forrest, S. R. Long-Range Absorption Enhancement in Organic Tandem Thin-Film Solar Cells Containing Silver Nanoclusters. *J. Appl. Phys.* **2004,** *96*, 7519–7526.
33. Chiu, T. L.; Xu, W. F.; Lin, C. F.; Lee, J. H.; Chao, C. C.; Leung, M. K. Optical and Electrical Characteristics of Ag-Doped Perylene Diimide Derivative. *Appl. Phys. Lett.* **2009,** *94*, 0133071–0133073.
34. Atwater., H. A.; Polman., A. Plasmonics for Improved Photovoltaic Devices. *Nat. Mater.* **2010,** *9*, 205–213.
35. Chen, F. C.; Chien, S. C.; Lee, S. W. High-Performance Single-Layer Polymer Electrophosphorescent Devices with Polymer Oxides. *Electrochem. Solid-State Lett.* **2008,** *11*, J50–J53.
36. Kim, K.; Carroll, D. L. Roles of Au and Ag Nanoparticles in Efficiency Enhancement of Poly(3-octylthiophene)/$C_{60}$ Bulk Heterojunction Photovoltaic Devices. *Appl. Phys. Lett.* **2005,** *87*, 2031131–2031133.
37. Li, G.; Shrotriva, V.; Huang, J.; Yao, Y.; Moriarty, T.; Emery, K.; Yang, Y. High-Efficiency Solution Processable Polymer Photovoltaic Cells by Self-Organization of Polymer Blends. *Nat. Mater.* **2005,** *4*, 864–868.
38. Varghese, O. K.; Crimes, C. A. Appropriate Strategies for Determining the Photoconversion Efficiency of Water Photoelectrolysis Cells: A Review with Examples Using Titania Nanotube Array Photoanodes. *Sol. Energy Mater. Sol. Cells* **2008,** *92*, 374–384.
39. Duret, A.; Grätzel, M. Visible Light-Induced Water Oxidation on Mesoscopic $\alpha$-$Fe_2O_3$ Films Made by Ultrasonic Spray Pyrolysis. *J. Phys. Chem. B* **2005,** *109*, 17184–17191.
40. Hummelen, J. C.; Kinght, B. W.; Lepeg, F.; Wuld, F.; Rao, J.; Wilkins, C. L. Preparation and Characterization of Fulleroid and Methanofullerene Derivatives. *J. Org. Chem.* **1995,** *60*, 532–538.
41. Sun, Y.; Yin, Y.; Mayers, B. T.; Herricks, T.; Xia, Y. Uniform Silver Nanowires Synthesis by Reducing $AgNO_3$ with Ethylene Glycol in the Presence of Seeds and Poly(Vinyl Pyrrolidone). *Chem. Mater.* **2002,** *14*, 4736–4745.